

Signatures of the bonding-antibonding splitting in the c -axis infrared response of moderately underdoped bilayer and trilayer cuprate superconductors


B. P. P. Mallett,^{1,2,3,*} P. Marsik,³ D. Munzar,⁴ C. Bernhard,³ and A. Dubroka^{4,†}

¹The Photon Factory, Department of Physics, The University of Auckland, 38 Princes St, Auckland 1010, New Zealand

²The MacDiarmid Institute for Advanced Materials and Nanotechnology, Victoria University of Wellington, PO Box 600, Wellington 6140, New Zealand

³University of Fribourg, Department of Physics and Fribourg Center for Nanomaterials, Chemin du Musée 3, CH-1700 Fribourg, Switzerland

⁴Department of Condensed Matter Physics, Faculty of Science, and Central European Institute of Technology, Masaryk University, Kotlářská 2, 61137 Brno, Czech Republic

 (Received 16 September 2018; revised manuscript received 28 January 2019; published 22 February 2019)

We report on results of our analysis of the c -axis infrared conductivity, $\sigma_c(\omega)$, of bilayer $\text{LnBa}_2\text{Cu}_3\text{O}_{7-\delta}$ (Ln=La, Nd, Y) and trilayer $\text{Bi}_2\text{Sr}_2\text{Ca}_2\text{Cu}_3\text{O}_{10+\delta}$ high- T_c superconductors. The analysis employs the multilayer model involving the conductivity of the bilayer or trilayer unit, $\sigma_{\text{bl}}(\omega)$, and that of the spacing layers separating the latter units, $\sigma_{\text{int}}(\omega)$. For the $\text{YBa}_2\text{Cu}_3\text{O}_{7-\delta}$ sample with concentration of holes $p = 0.09$, our fitting of the data strongly suggests that at low temperatures, the conductivity $\sigma_{\text{bl}}(\omega)$ possesses a pronounced and narrow Drude peak. For samples with $p \geq 0.115$ however, the fitting indicates that $\sigma_{\text{bl}}(\omega)$ is, at low temperatures, dominated by a mode at a finite energy in the range from 30 to 60 meV. The properties of this resonance are in accord with those of a collective mode that appears in the spectra of $\sigma_{\text{bl}}(\omega)$ calculated using a microscopic gauge-invariant theory of $\sigma_c(\omega)$ by J. Chaloupka and coworkers [*Phys. Rev. B* **79**, 184513 (2009)]. The frequency and spectral weight of the latter mode are determined by the magnitude of the splitting between the bonding and the antibonding band of the bilayer or trilayer unit. Our results, in conjunction with the microscopic theory, thus demonstrate that in moderately underdoped bilayer and trilayer high- T_c cuprates the bilayer (or trilayer) splitting is already developed. The observed doping dependence is consistent with results from angular resolved photoemission spectroscopy.

DOI: [10.1103/PhysRevB.99.054513](https://doi.org/10.1103/PhysRevB.99.054513)

I. INTRODUCTION

The c -axis infrared (IR) response of high- T_c cuprate superconductors contains a wealth of information that includes the temperature and energy scales of the pseudogap and the superconducting (SC) gap [1–8]. In materials with two CuO_2 layers per unit cell (the so-called bilayer compounds), the c -axis response also reflects the electronic coupling within the pairs of closely spaced CuO_2 layers. This coupling gives rise to a broad absorption peak in the spectra of the real part of the c -axis conductivity $\sigma_c(\omega)$, located in the frequency region between 350 cm^{-1} and 550 cm^{-1} [9,10]. The peak, labeled as the transverse plasmon mode (TPM) in the following, onsets at a temperature T^{ons} that, in underdoped cuprates, is higher than T_c but lower than the temperature scale, T^* , associated with the pseudogap [7]. The formation of the TPM is accompanied by pronounced changes of the spectral structures corresponding to some infrared-active phonons—the so-called phonon anomalies. These anomalies are well understood in terms of a coupling of the phonons to charge density oscillations between the closely spaced layers connected with the TPM. Despite the fact that the anomalies

do not give evidence for a phonon-mediated mechanism of superconductivity, they represent a very sensitive probe of the low-energy charge excitations. This sensitivity was used to track the anomalous temperature dependence of the TPM in underdoped $\text{YBa}_2\text{Cu}_3\text{O}_{7-\delta}$ (Y123), in particular its onset, far above T_c in strongly underdoped samples, that was interpreted in terms of superconducting or pairing fluctuations [7,8]. In addition, the TPM and the anomalies have gained considerable interest in the context of possible optical enhancement of superconductivity [11–13].

The TPM and the phonon anomalies in strongly underdoped samples have been modelled [7,14–16] successfully by an extension of the so-called multilayer model (MLM) originally proposed in Ref. [17]. Here, the bilayer cuprates are thought of as consisting of layers with distinctively different electronic properties. In particular, the layer limited by the closely spaced copper-oxygen layers—the so-called intrabilayer region—is much more conducting than the layer separating the bilayer blocks—the so-called interbilayer region. The conductivities of the former and of the latter will be denoted as $\sigma_{\text{bl}}(\omega)$ and $\sigma_{\text{int}}(\omega)$, respectively. The TPM can be interpreted in terms of resonant oscillations of the charge density between the closely spaced CuO_2 layers, enabled by the difference between $\sigma_{\text{bl}}(\omega)$ and $\sigma_{\text{int}}(\omega)$. These charge oscillations are infrared active and give rise to strong modifications of the local fields acting on the ions that participate in the phonon

*benjamin.mallett@gmail.com

†dubroka@physics.muni.cz

modes. This causes the phonon anomalies. It was indeed shown that the MLM provides an excellent description not only of the TPM but also of the phonon anomalies in the strongly underdoped cuprates [7,14,15]. In these studies it was assumed that the intrabilayer conductivity $\sigma_{\text{bl}}(\omega)$ responsible for the TPM has its transverse frequency at zero, i.e., its spectra are similar to those of the bulk Drude response. However, it was suggested earlier [18] that the TPM could be related to the transitions between the bonding and antibonding bands of bilayer cuprates which can occur in the coherent limit relevant for higher dopings. The suggestion of Dordevic *et al.* [18] implicitly involves the idea that $\sigma_{\text{bl}}(\omega)$ has a finite transverse frequency [i.e., $\sigma_{\text{bl},1}(\omega)$ displays a maximum at a finite frequency]. More recently, detailed microscopic calculations of the c -axis response were performed by some of us using a nonperturbative approach involving the bilayer split bands [19]. These calculations, which are relevant for the limit of two well developed bands, showed that the transverse frequency of $\sigma_{\text{bl}}(\omega)$ indeed does not occur at zero but at a finite frequency. Early angular resolved photoemission spectroscopy (ARPES) experiments had failed to resolve a bilayer splitting of the conduction band and it was not until overdoped $\text{Bi}_2\text{Sr}_2\text{CaCu}_2\text{O}_{8-\delta}$ (Bi2212) samples were measured that the bonding and antibonding bands were individually resolved [20–22]. More recently, splitting between the two bands was observed by ARPES in optimally doped $\text{Bi}_2\text{Sr}_2\text{Ca}_2\text{Cu}_3\text{O}_{10-\delta}$ (Bi2223) [23] and in $\text{YBa}_2\text{Cu}_3\text{O}_{7-\delta}$ (Y123) [24–26].

Inspired by these findings, we seek to discern the effect of the conduction band splitting in the c -axis response of several moderately underdoped cuprates. We study $\text{LnBa}_2\text{Cu}_3\text{O}_{7-\delta}$ ($\text{Ln}=\text{Y},\text{Nd},\text{La}$) with hole doping from $p \approx 0.1$ to 0.16 and the Bi2223 trilayer cuprate superconductor. We use the MLM scheme to fit our data and allow the local intrabilayer conductivity $\sigma_{\text{bl}}(\omega)$ to be either centered at zero or at a finite frequency, i.e., to model negligible or significant bonding-antibonding splitting, respectively. We show here that the model with the finite transverse frequency of $\sigma_{\text{bl}}(\omega)$ indeed yields significantly better fits to the data for moderately underdoped samples ($p \geq 0.115$). This provides evidence for bonding-antibonding splitting of the conduction band in the bulk for bi- and trilayer cuprates.

II. METHODS

A. Samples and measurements

The high quality twinned $\text{R}\text{Ba}_2\text{Cu}_3\text{O}_{7-\delta}$ ($R=\text{La}, \text{Nd},$ and Y) crystals were flux grown in Y-stabilized zirconium crucibles. For $R=\text{Nd}$, the crystals were grown under reduced oxygen atmosphere to avoid spurious substitution of the Nd ion onto the Ba site [27]. The crystals were annealed, while covered in $\text{YBa}_2\text{Cu}_3\text{O}_{7-\delta}$ (Y123) powder to protect their surfaces, in a pure oxygen atmosphere at various temperatures in order to alter δ and hence the electronic doping of the CuO_2 layers. When necessary the crystals were mechanically polished to optical grade using diamond powder paste, however, virgin surfaces were used where possible. The typical c -axis dimension of our Y123 single crystals was 0.5 to 1 mm. Since the c -axis response is insulatorlike, the diffraction effects are much less pronounced than for the metallic in-plane response.

For the c -axis response of these Y123 crystals, diffraction effects set in gradually with decreasing wave number and become noticeable below about 200 cm^{-1} where they mainly cause a decrease of the spectral weight of the phonons. The c -axis dimensions of the Nd123 and La123 crystals are about 2 mm and thus the diffraction sets in at even lower frequencies than for the Y123 crystals.

The c -axis IR response was measured using broadband ellipsometry. Ellipsometry is a self-normalizing optical technique to directly measure the complex conductivity, $\sigma(\omega) = -i\epsilon_0\omega[\epsilon(\omega) - 1]$, without the need for a Kramers-Kronig analysis [28]. We used an in-house built ellipsometer attached to a Bruker fast-Fourier spectrometer at the infrared beam line of the ANKA synchrotron at the Karlsruhe Institute for Technology (KIT) to measure in the far-IR range from 70 cm^{-1} to 700 cm^{-1} , see Ref. [29], and a similar laboratory-based setup at University of Fribourg covering the far-IR to mid-IR range, 100 cm^{-1} to 4500 cm^{-1} . For these ellipsometry measurements we used a rotating analyzer configuration and anisotropy corrections were performed where necessary using standard numerical procedures [28,29].

B. Multilayer model fitting

We have analyzed our data with the MLM [14] whose details have been described previously and we use here the same structure of the interaction between the phonons and the electronic degrees of freedom as in Refs. [16,30]. For clarity however, we repeat a few key expressions below. The c -axis response in the optical limit is written as a sum of volume-averaged (microscopic) current densities, $\langle j_k(\omega) \rangle$:

$$\epsilon(\omega) = \epsilon_\infty + \frac{i}{\epsilon_0\omega} \frac{\sum_k \langle j_k(\omega) \rangle}{E(\omega)}. \quad (1)$$

Here, ϵ_∞ is the high frequency dielectric constant (a fitted parameter) and $E(\omega)$ the total electric field along the c axis. Next, the expression above is expanded as follows:

$$\begin{aligned} \epsilon(\omega) = & \epsilon_\infty \\ & + \frac{d_{\text{bl}}}{d_{\text{bl}} + d_{\text{int}}} \frac{i}{\epsilon_0\omega} \frac{j_{\text{bl}}(\omega)}{E(\omega)} + \frac{d_{\text{int}}}{d_{\text{bl}} + d_{\text{int}}} \frac{i}{\epsilon_0\omega} \frac{j_{\text{int}}(\omega)}{E(\omega)} \\ & + \chi_{\text{int}}^Q(\omega) \frac{E_{\text{int}}^{\text{loc}}(\omega)}{E(\omega)} + \chi_{\text{ocp}}^Q(\omega) \frac{E_{\text{ocp}}^{\text{loc}}(\omega)}{E(\omega)} + \chi_{\text{Lor}}^Q(\omega). \end{aligned} \quad (2)$$

The second and the third terms represent the contributions of the intrabilayer and interbilayer current densities, denoted by “bl” and “int,” respectively. The fourth, fifth, and sixth terms describe the contributions of phonons driven by the local fields, $E_{\text{int}}^{\text{loc}}(\omega)$, of the interbilayer region, $E_{\text{ocp}}^{\text{loc}}(\omega)$ acting on the (outer) CuO_2 layers and by the average electric field, $E(\omega)$, respectively. The last term includes standard Lorentz phonon lineshapes corresponding to noninteracting (mean field) phonons. The intrabilayer and interbilayer current densities are given by the corresponding averaged local fields and local conductivities:

$$j_{\text{bl}}(\omega) = \sigma_{\text{bl}}(\omega)E_{\text{bl}}(\omega), \quad (3)$$

$$j_{\text{int}}(\omega) = \sigma_{\text{int}}(\omega)E_{\text{int}}(\omega). \quad (4)$$

The conductivities are represented in terms of the corresponding polarizabilities, $\chi_{\text{bl}}(\omega)$ and $\chi_{\text{int}}(\omega)$, as $\sigma_{\text{bl}}(\omega) = -i\omega\epsilon_0\chi_{\text{bl}}(\omega)$ and $\sigma_{\text{int}}(\omega) = -i\omega\epsilon_0\chi_{\text{int}}(\omega)$. Drude-Lorentz terms are used to describe components of all the polarizabilities involved (χ_{bl} , χ_{int} , χ_{int}^O , χ_{ocp}^O , and χ_{Loc}^O), each of them is expressed as

$$\chi(\omega) = \sum_m \frac{\omega_{\text{pl},m}^2}{\omega_{0,m}^2 - \omega^2 - i\omega\gamma_m} \quad (5)$$

with the resonant frequency $\omega_{0,m}$ being either finite or zero for a Lorentz or Drude term, respectively. Detailed formulas for the averaged local fields [e.g., $E_{\text{bl}}(\omega)$] and the local fields acting on the ions [e.g., $E_{\text{ocp}}^{\text{loc}}(\omega)$] are given in Ref. [30].

In summary, the MLM represents a set of self-consistent equations describing the coupling between the lattice vibrations and the local current densities via electrostatic interaction. The equations can be derived starting from a fully microscopic theory involving Green's function [31]. As a result, phonon anomalies, such as an asymmetrical line shape or atypical temperature dependence, can be accounted for as a consequence of changes in $\sigma_{\text{bl}}(\omega)$ and/or $\sigma_{\text{int}}(\omega)$.

III. DATA AND ANALYSIS

A. $\text{YBa}_2\text{Cu}_3\text{O}_{6.65}$ with $p = 0.115$

To demonstrate how a bilayer splitting may be discerned from IR spectroscopy data, we focus first on an underdoped Y123 sample with $T_c = 75$ K and $p = 0.115$. Figure 1(a) shows the real and imaginary parts of the c -axis IR conductivity measured at 120 K (red lines) and 10 K (cyan lines). The spectra display six IR active phonon modes and an electronic background. The largest changes with cooling to 10 K occur between 250–700 cm^{-1} where the broad band centered at 480 cm^{-1} —the TPM—emerges and the phonon peaks at 190, 280, 320, 560, and 630 cm^{-1} exhibit sizable spectral changes. The latter effects are the well known phonon anomalies that were recognized and extensively studied earlier [4,5,7,14,32].

In order to quantitatively analyze the data, we use the MLM with the same assumptions as in our earlier studies, i.e., the phonons at 280, 560, 630 cm^{-1} that involve vibrations of the apical and chain oxygen are driven by the local field $E_{\text{int}}^{\text{loc}}(\omega)$ and the phonon at 320 cm^{-1} that involves vibrations of the planar oxygens is driven by the local field $E_{\text{ocp}}^{\text{loc}}(\omega)$. The only difference as discussed below is that we show how the model spectra fit the data in two different cases: (a) if the resonance frequency of $\chi_{\text{bl}}(\omega)$ is fixed at zero and (b) if it is allowed to be finite. The two low frequency phonons at 155 and 190 cm^{-1} are treated as mean field phonons whose parameter values are fitted at each temperature. Note that the 190 cm^{-1} phonon peak, although its spectral weight is small exhibits sizable anomaly as well: The spectral weight increases significantly when going from the normal to the superconducting state. This anomaly is related to the temperature dependence of the intrabilayer local field and to the complex polarization

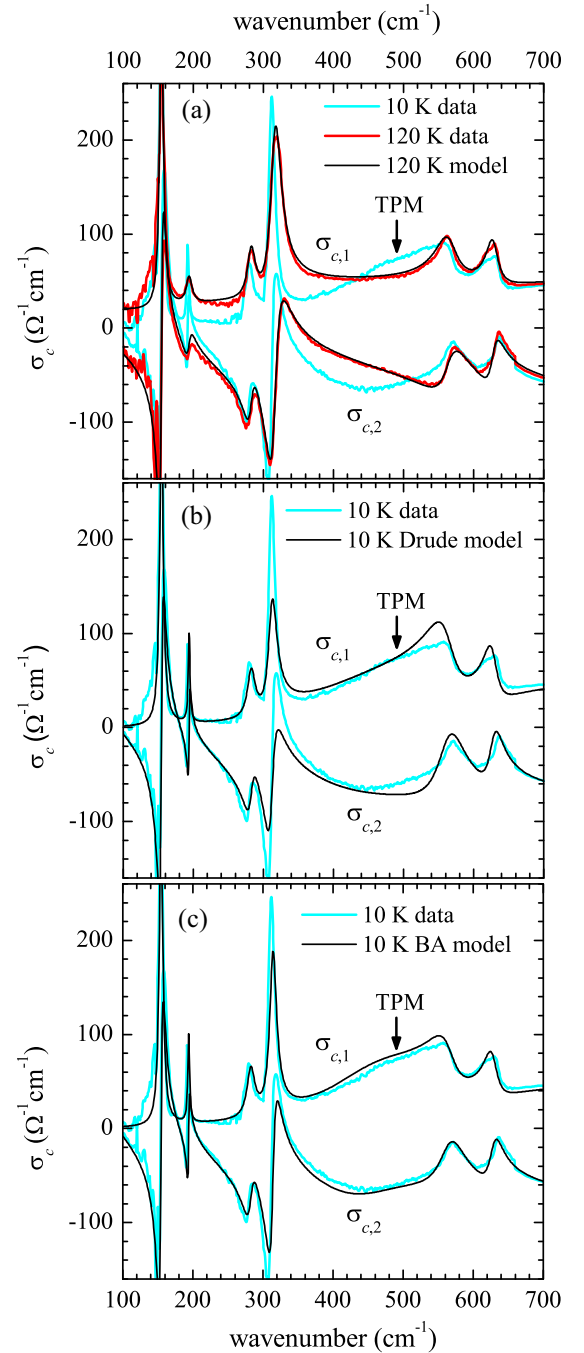


FIG. 1. The real and imaginary parts of the c -axis conductivity, $\sigma_{c,1}(\omega)$ and $\sigma_{c,2}(\omega)$, for the Y123 sample with $p = 0.115$ at 120 K (red lines) and 10 K (cyan lines). The panels show also the fitted spectra obtained using the MLM (black lines) for (a) 120 K, (b) for 10 K with $\sigma_{\text{bl}}(\omega)$ described using the Drude model, and (c) for 10 K with $\sigma_{\text{bl}}(\omega)$ described using the BA model. The arrow shows the center frequency of the transverse plasma mode (TPM).

diagram of the phonon [16].¹ Its description is beyond the scope of this paper.

¹The eigenvector of the 190 cm^{-1} phonon in Y123 involves mainly the in-phase motion of yttrium and planar oxygen ions, see Ref. [45]. However, since the effective charge of oxygen is negative and that

A key feature of our fitting is that the values of the parameters of the phonons driven by the local fields (the four phonons above 250 cm^{-1} in the case of Y-123) are obtained by fitting the data above T_c (usually at 120 K) and are then kept fixed when fitting the data sets corresponding to lower temperatures. This leaves only variations in $\sigma_{\text{bl}}(\omega)$ [and $\sigma_{\text{int}}(\omega)$] to describe the low temperature electronic response, the TPM, and the phonon anomalies. Consequently, the spectra of $\sigma_{\text{bl}}(\omega)$ and $\sigma_{\text{int}}(\omega)$ are well determined. Both real and imaginary parts of the conductivity, $\sigma_{c,1}(\omega)$ and $\sigma_{c,2}(\omega)$, are used for fitting up to 4000 cm^{-1} (except for the Bi-based cuprates for which we only have the data up to 700 cm^{-1}). This reduces ambiguities in the determination of the local conductivities.

The black lines in Fig. 1(a) show the fit of the MLM to the data for 120 K. At this doping, the values of the oscillator parameters of the 320 cm^{-1} phonon are $\omega_{\text{pl}} = 460\text{ cm}^{-1}$ and $\omega_0 = 410\text{ cm}^{-1}$. The values of the two frequencies are very similar to those of a Y123 sample with $T_c = 58\text{ K}$ and $p = 0.09$ obtained using the MLM model recently [7]. Values of all the parameters are tabulated in Table I.

When applying the MLM to the low temperature data, we find that it is the form of the intrabilayer conductivity, $\sigma_{\text{bl}}(\omega)$, rather than the interbilayer conductivity, $\sigma_{\text{int}}(\omega)$, that determines the shape of the TPM. We first assume that the main contribution to $\sigma_{\text{bl}}(\omega)$ in the far-IR frequency range is given by a Drude peak with $\gamma = 0$. Previously, such a model was successfully used in fitting the data of the strongly underdoped Y123 sample with $T_c = 58\text{ K}$ [7,14]. The model with this assumption will be denoted as the ‘‘Drude model’’ and the corresponding fits are shown in Fig. 1(b) using the black lines. Although the Drude model based fits for our $p = 0.115$ K sample capture the main trends in the spectra, there are significant deviations: (i) the spectral weight of the phonons at 560 and 630 cm^{-1} is overestimated, (ii) the TPM feature does not have a convex (bellylike) shape but rather a concave shape, and finally (iii) the spectral weight of the 320 cm^{-1} phonon is too low.

Next, we relax our earlier assumption and allow the main contribution to the intrabilayer conductivity $\sigma_{\text{bl}}(\omega)$ in the far-IR range to be centered at a finite frequency. We have labeled this approach as the ‘‘BA model,’’ motivated by the similarity between the corresponding mode of the microscopic theory of Ref. [19] (‘‘BA mode’’) and the Bogolyubov-Anderson mode of a single layer superconductor. Figure 1(c) and, over an extended spectral range, Fig. 2(a) show the corresponding model spectra where the resonance of $\chi_{\text{bl}}(\omega)$ is centered at about 260 cm^{-1} and the Drude peak with $\gamma = 0$ is absent, as shown in Fig. 2(b) which displays the local conductivities. It is clear that this model fits the data much better in all three aspects

of yttrium positive, the corresponding polarization pattern of the eigenvector has an out-of-phase character. It was shown that an out-of-phase resonance of ions in the outer CuO_2 layers and in the intrabilayer region is strongly enhanced in the superconducting state if it is located at lower frequency than that of the TPM, see Fig. 8(a) in Ref. [16]. We believe that this is the main cause for the observed strong enhancement of the phonon at 190 cm^{-1} in Y123. The phonon at 400 cm^{-1} in Bi2223 is anomalous for similar reasons, see Sec. C.

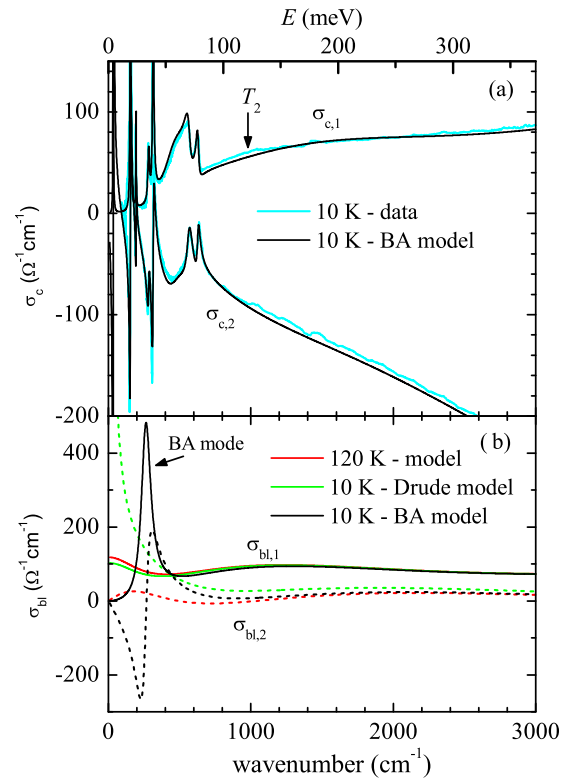


FIG. 2. Panel (a) shows the 10 K data for the Y123 sample with $p \approx 0.115$ (cyan lines) and the MLM model based fit (black lines) over an extended spectral range. (b) The real (solid lines) and imaginary (dotted lines) parts of the local intrabilayer conductivity $\sigma_{\text{bl}}(\omega)$ involved in the fits shown in Fig. 1 and in panel (a).

for which the Drude model failed. Particularly the bellylike shape of the TPM feature and the phonon anomalies of the 560 and 630 cm^{-1} phonons are significantly better reproduced. We note however that a weak Drude term in $\sigma_{\text{bl}}(\omega)$, i.e., a weak SC delta function in the real part of $\sigma_{\text{bl}}(\omega)$, with a spectral weight much smaller than that of the finite frequency mode, would not be inconsistent with the present fit in the region of the TPM. Consequently we do not claim that the SC delta function is completely absent, we just claim that the main cause for the observed TPM and the phonon anomalies at this doping is the finite frequency mode and not the SC delta function. Actually, a weak SC delta function, with the plasma frequency comparable to that of $\sigma_{\text{int}}(\omega)$ (see Table I), must be present also in $\sigma_{\text{bl}}(\omega)$ for the whole multilayer structure to exhibit a dc superconducting response.

Next, we discuss in more detail the spectra of $\sigma_{\text{bl}}(\omega)$ obtained from the fits, which are shown in Fig. 2(b). First, we can see that the high frequency part above 1000 cm^{-1} is essentially temperature and model independent with the major changes occurring at lower frequencies. At 120 K, the response is essentially incoherent with a broad Drude term with the plasma frequency $\omega_{\text{pl}} = 1400\text{ cm}^{-1}$ and the broadening parameter $\gamma = 280\text{ cm}^{-1}$. Considering the width of the Drude term, the question as to whether the resonance is at zero or at small finite frequency cannot be answered.

The solid green line in Fig. 2(b) represents the spectrum of $\sigma_{\text{bl},1}(\omega)$ corresponding to the Drude model based fit for

TABLE I. Values of the fitting parameters entering the model formulas: frequencies (ω_0), plasma frequencies (ω_{pl}), and broadening parameters (γ) of the oscillators obtained by fitting the high temperature (100–160 K) and the 10 K data of Ln123 crystals. All values of phonon parameters have been obtained by fitting the high temperature data and fixed for 10 K fitting except for some phonon parameters of Y123 with $p = 0.09$ that were allowed to vary to accommodate for the large temperature difference analyzed in Ref. [7].

p	Y123								La123		Nd123	
	0.09		0.115		0.124		0.137		0.12		0.12	
T_c (K)	58		75		82		87		87		84	
T (K)	160	10	120	10	140	10	120	10	100	10	120	10
ϵ_∞	4.30	4.30	4.05	4.05	3.86	3.71	3.97	3.82	3.88	3.88	3.70	3.63
σ_{bl} oscillators (cm^{-1})												
ω_0	0	0	0		0		0		0		0	
ω_{pl}	1520	400	1416		621		1902		1548		851	
γ	150	150	283		1385		446		869		37	
ω_0		0		264	303	387		439		218	650	354
ω_{pl}		1830		1496	1146	1476		1157		1178	2555	1010
γ		0		80	250	129		140		157	2650	107
ω_0	1760	1777	1251	1250	1331	2000	1735	1700	3200	2200	800	1280
ω_{pl}	5900	5900	3748	3748	3809	6561	4431	4635	3360	4109	1010	2689
γ	3750	3670	2680	2700	3600	3600	3100	3000	3500	3500	1340	2650
ω_0	3000	3000	7000	7000	6090	6000	6000	6000	8000	8000	7200	7200
ω_{pl}	3470	3530	6617	6617	6410	8519	5680	5588	2696	4547	5631	5831
γ	3330	3300	8690	8000	9000	9000	6300	7000	7000	7000	6700	6700
σ_{int} oscillators (cm^{-1})												
ω_0	0	0	0	0	0	0	0	0	0	0	0	0
ω_{pl}	340	274	380	380	2039	659	15	811	1630	667	1433	650
γ	300	300	70	0	1334	0	600	0	1550	50	1920	0
ω_0		0				952						
ω_{pl}		195				1303						
γ		0				1070						
ω_0	1500	1730	1654	2500	2080	1500	685	1050	1400	1100	1400	1400
ω_{pl}	2950	2950	4657	4657	4127	3852	3980	3626	3147	2568	4070	4077
γ	5140	5210	9154	9000	5160	5500	3000	3000	2227	1800	2600	2600
ω_0	3000	3000	7000	7000	5500	5500	7000	7000	7000	7000	6500	6500
ω_{pl}	2150	2180	9213	9213	6007	4634	10000	10000	12430	12430	9034	9413
γ	2960	3200	8340	8300	5500	5500	5300	5300	6200	6200	7000	7000
Planar oxygen phonon modes (cm^{-1})												
ω_0	410	410	410		408		401		407		411	
ω_{pl}	481	481	460		441		426		430		450	
γ	24	31	9.6		12.3		8.9		24.4		8.2	
Inter-bilayer phonon modes (cm^{-1})												
ω_0	286	282	288		288		288		280		288	
ω_{pl}	44	45	53.9		53.9		55.0		22.6		77.3	
γ	13	9	14.8		14.8		13.4		12.4		45.2	
ω_0	558	564	589		600		604		0		611	
ω_{pl}	132	132	247		265		207		0		157	
γ	24	32	30.7		24.6		16.4		0		21.1	
ω_0	650	650	652		644		650		668		640	
ω_{pl}	294	263	378		372		457		504		483	
γ	17	14	14		9.6		8.8		7.7		22	

10 K. It looks very similar to the one of $T = 120$ K, however it has a delta function at zero frequency with quite a significant plasma frequency of $\omega_{pl} = 1400 \text{ cm}^{-1}$ giving rise to the low-frequency upturn in $\sigma_{bl,2}(\omega)$. The solid black line represents the spectrum corresponding to the BA model at 10 K. It exhibits a sharp mode centered at 260 cm^{-1} with a plasma frequency of about 1500 cm^{-1} , to be labeled

as BA mode in the following. Note that the frequency of the BA mode is significantly lower than 470 cm^{-1} , the frequency of the TPM. This is because the TPM occurs close to the screened longitudinal frequency of the intrabilayer response that is determined by both the transverse frequency and the spectral weight of the BA mode, for details see Appendix.

B. Interpretation of the BA mode

The properties of the peak in $\sigma_{\text{bl},1}(\omega)$ discussed above are well comparable to those of the BA mode occurring in the spectra of $\sigma_{\text{bl}}(\omega)$ reported in Ref. [19], obtained using a microscopic gauge-invariant theory involving the bilayer-split (bonding and antibonding) bands; see Figs. 10(d) and 14(a) of Ref. [19], in particular the spectra corresponding to $t_{\perp} = 45$ meV in Fig. 10(d) and $t_{\perp} = 30$ meV in Fig. 14(a). Here t_{\perp} is the intrabilayer hopping parameter.

1. Bogolyubov-Anderson mode

The nature of the BA mode of Ref. [19] is similar to that of the Bogolyubov-Anderson mode that participates in the longitudinal response of a homogeneous superconductor. We recall that in homogeneous superconductors a longitudinal electromagnetic field excites the Bogolyubov-Anderson mode involving density fluctuations of the electron system, associated with a modulation of the phase of the order parameter [33–35]. The energy of the Bogolyubov-Anderson mode is proportional to $v_F|\mathbf{q}|$, where v_F is the Fermi velocity and \mathbf{q} the wave vector. So far we did not consider the Coulomb interaction between the carriers, that will shift the mode towards higher frequencies. In a single-layer superconductor (one CuO_2 plane per unit cell), a longitudinal electromagnetic field with $\mathbf{E} \parallel c$ would induce a Bogolyubov-Anderson-like mode with energy proportional to the Fermi velocity along the c axis. Again the Coulomb interaction shifts the mode towards higher frequencies. In the long-wavelength limit we obtain the c -axis plasma mode.

2. Relation between the BA mode and the Bogolyubov Anderson mode

In the present case of the IR response of a bilayer superconductor the situation is more complicated. The electromagnetic wave is transverse with $\mathbf{q} \perp c$. Nevertheless, it induces a charge density that is modulated along the c axis. For small values of t_{\perp} the modulation is accompanied by oscillations of the relative phase of the two planes, see Fig. 4(b) of Ref. [19]. The pattern is analogous to the one associated with the Bogolyubov-Anderson mode of a single-layer superconductor with $\mathbf{q} \parallel c$, $|\mathbf{q}| = \pi/d$ shown in Fig. 4(a) of Ref. [19]. The analogy allows us to interpret the BA mode of σ_{bl} as an analog of the Bogolyubov-Anderson mode. This point of view can be substantiated by comparing the equations describing the modes as detailed in Ref. [19]. Note that the long-wavelength in-plane modulation of the electromagnetic wave has qualitatively no impact on the mode. In the total conductivity the BA mode is shifted to higher energies by the interlayer Coulomb interaction. The resulting structure corresponding as we believe to the TPM is labeled as T_1 in Ref. [19].

3. Relation between the energy of the BA mode and the bonding-antibonding splitting

Note that the energy of the BA mode is proportional to t_{\perp} , i.e., to the bilayer splitting (the unrenormalized magnitude of the band splitting is $2t_{\perp}$). It has been argued by Hirata *et al.* [36] that the strong temperature dependence of the TPM mode

in multilayer Hg-based cuprates below T_c indicates that the mode is rather due to the plasma of the superconducting pairs than to an interband transition. We agree that the temperature dependence suggests that superconductivity is a prerequisite for the formation of the TPM. But in addition there is, we believe, a relation to the bonding-antibonding splitting that we explain below. According to the model of Ref. [19] the normal state spectra of $\sigma_{\text{bl},1}(\omega)$ display a very broad band that can be roughly interpreted as an overdamped interband bonding-antibonding transition, see Fig. 10(b) of Ref. [19]. In the total conductivity the resulting structure is even broader, see Fig. 10(e) of Ref. [19]. In the superconducting state, however, the band in $\sigma_{\text{bl},1}(\omega)$ becomes fairly narrow, see Fig. 10(d) of Ref. [19]. A sharp band shifted to higher energies appears then in the spectra of the total conductivity, see Fig. 10(f) of Ref. [19]. The important questions are: (a) Why is the energy of the band in the superconducting state unrelated to the superconducting energy gap Δ ? (b) Why is the band so narrow?

Regarding (a): the infrared radiation excites quasiparticles. A typical final state—in the absence of interactions—would involve a Bogolyubov quasiparticle of the bonding band (energy $E_b = \sqrt{\Delta_b^2(\mathbf{k}) + \epsilon_b^2(\mathbf{k})}$) and a Bogolyubov quasiparticle of the antibonding band (energy $E_a = \sqrt{\Delta_a^2(\mathbf{k}) + \epsilon_a^2(\mathbf{k})}$). Here Δ_b and Δ_a are the superconducting gaps of the two bands and ϵ_b and ϵ_a the corresponding dispersions. The total energy of the excited state would be $E_b(\mathbf{k}) + E_a(\mathbf{k})$. The excited quasiparticles however interact and form a bound state (this is similar to the formation of an exciton below the band gap of a semiconductor), whose energy is determined by t_{\perp} rather than by Δ .

Regarding (b): The band is so narrow because the quasiparticle background is strongly suppressed by the formation of the superconducting gap. As the band moves into the quasiparticle continuum above 2Δ , it becomes fairly broad, see Figs. 10(d) and 10(f) of Ref. [19].

These facts explain the rapid development below T_c of the band inside the superconducting gap. Note that for small values of the bilayer splitting, the nature of the BA mode is very similar to that of the bilayer plasmon of the phenomenological Josephson superlattice model used in many earlier studies.

4. Pair breaking bonding-antibonding transition

We have stressed that the BA mode and the TPM cannot be simply interpreted in terms of a transition between the bonding and the antibonding bands. Such a transition (a pair-breaking bonding-antibonding transition) is predicted to occur somewhat above the superconducting gap and indeed a second superconductivity-induced mode appears in the data at higher frequencies [19]. For our Y123 sample with $p = 0.115$, the latter mode occurs at about 120 meV and it is denoted as T_2 in Fig. 2(a). Next we address the nature of this second mode. In our discussion of the energy of the BA mode above, we have mentioned final states with energy $E_b(\mathbf{k}) + E_a(\mathbf{k})$. In the expressions for σ_{bl} they are coupled and yield a bound state (excitonlike) inside the superconducting gap. In the expression for σ_{int} they are not coupled because there are, within the model, no interactions between different bilayers.

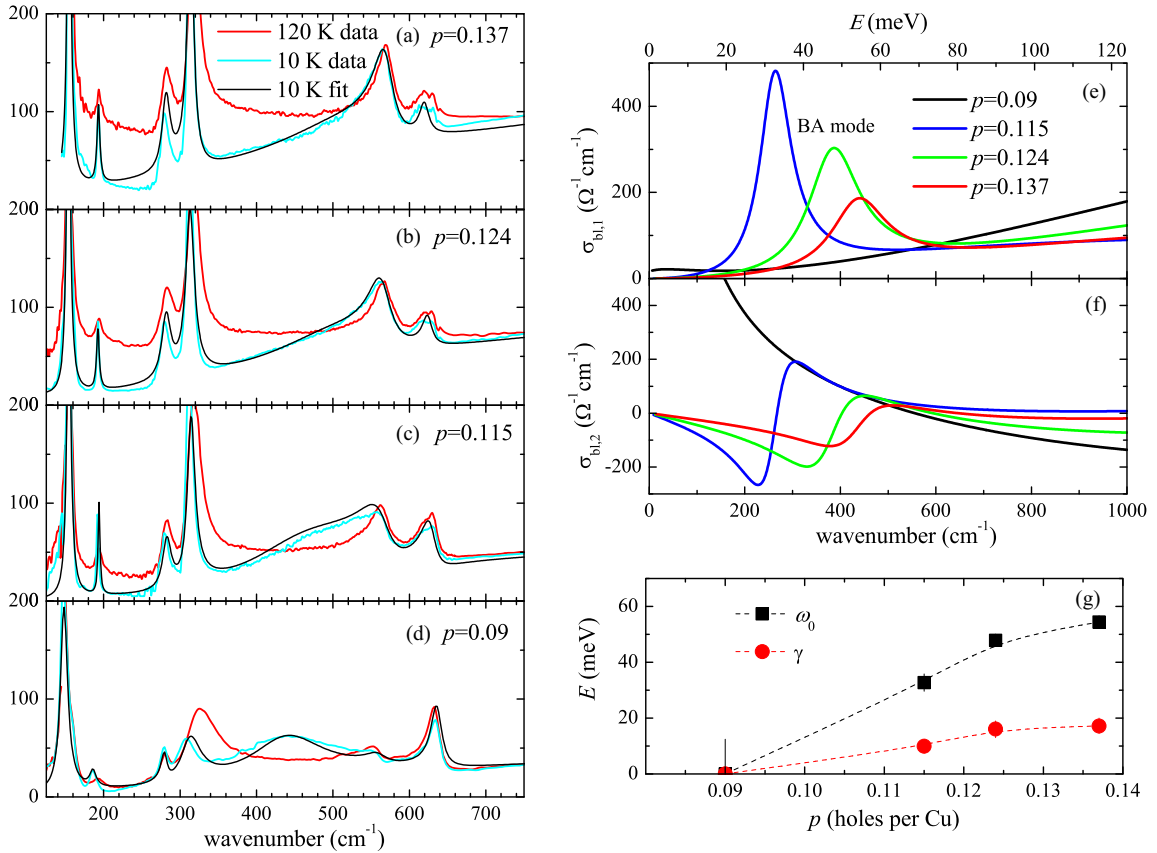


FIG. 3. Doping dependence of the BA mode in Y123. Panels (a)–(d) show the $T = 10$ K spectra of $\sigma_{c,1}(\omega)$ (cyan lines) and the 120 K spectra (red lines) for Y123 with various values of the doping p . The black lines are fits of the 10 K data obtained using the MLM. Panels (e) and (f) show the real and imaginary parts of $\sigma_{bl}(\omega)$, respectively, inferred from the MLM fitting for 10 K. Panel (g) shows the doping evolution of the BA mode’s frequency, ω_0 , and its broadening parameter γ . The lines are guides to the eye.

These final states give rise to a structure somewhat above 2Δ , see Fig. 13 of Ref. [19]. The energy is above 2Δ because of the factors $\epsilon_b(\mathbf{k})$ and $\epsilon_a(\mathbf{k})$ in $E_b(\mathbf{k})$ and $E_a(\mathbf{k})$ that cannot be simultaneously zero.

C. Doping and intralayer distance dependence

Here we address the doping and intralayer distance dependencies of the BA mode inferred from our MLM fitting and compare it with expectations based on theory and ARPES measurements. Figures 3(a)–3(d) shows $\sigma_{c,1}(\omega)$ data for Y123 with p ranging from 0.137 to 0.09, along with the corresponding fits obtained using the MLM. We use the same version of the MLM here for all doping values—we only vary the values of the fitting parameters that are listed in Table I.

In the case of the strongly underdoped sample with $p = 0.09$, the best fit is obtained using the Drude model, see Fig. 3(d). The model with the frequency of the BA mode in the range 150–300 cm⁻¹ led to worse agreement with the data (not shown). Note that based on the data it cannot be decided whether the resonance of $\sigma_{bl}(\omega)$ is located at $\omega = 0$ or at a finite ω smaller than about 100 cm⁻¹ because the differences between the fits are not significant.

With increasing doping, the TPM moves to higher energies where it eventually merges with the continuum for $p \approx 0.15$ in Y123 [30]. Meanwhile, the associated phonon anomalies

become progressively weaker. As the TPM and the anomalies become less pronounced, the results of the MLM analysis become less reliable. The highest doping for which we were able to perform a reliable MLM based data analysis is $p = 0.137$ for Y123 with $T_c = 87$ K [see Fig. 3(a)] and $p \approx 0.145$ for Nd123 with $T_c = 94$ K (the effects of the substitution of Nd for Y are addressed below). Figures 3(e) and 3(f) display the inferred real and imaginary parts of $\sigma_{bl}(\omega)$, respectively, for the Y123 series. For $p \geq 0.115$ the spectra exhibit a BA mode at a finite energy instead of a Drude peak. The energy, ω_0 , and broadening, γ , of this mode increases with increasing doping, as shown in Fig. 3(g). Our results, in conjunction with the microscopic theory of Ref. [19], indicate that the bonding-antibonding splitting develops for p above the critical value of 0.10 ± 0.01 . The observed increase of ω_0 with increasing p is consistent with the assumption that the effective value of the intralayer hopping matrix element t_{\perp} increases with doping (it has been shown in Ref. [19] that the energy of the BA mode increases with t_{\perp} and the same applies to the T_1 mode corresponding to the TPM).

ARPES experiments on Y123 samples with the surface doping controlled through *in situ* deposition of K atoms reveal a collapse of the bonding and antibonding Fermi surfaces into four nodal Fermi arcs for doping levels below $p_c = 0.12 \pm 0.02$ [24,25]. Our results agree within the error bars with this value and suggest that the collapse occurs likely

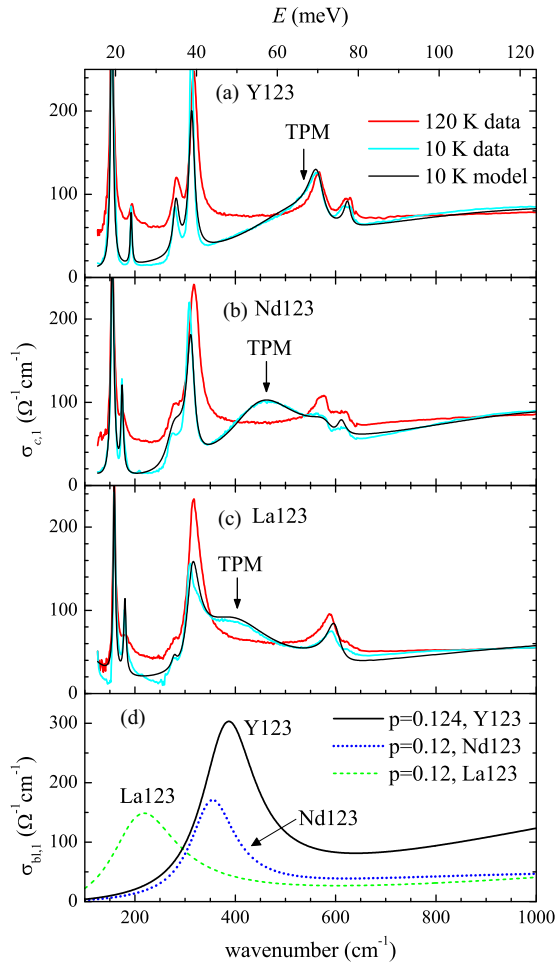


FIG. 4. Intralayer distance dependence of the BA mode. Panels (a), (b), and (c) show the $\sigma_{c,1}(\omega)$ spectra at $T = 10$ K (cyan lines) and at 120 K (red lines) for $p \approx 0.12$ Ln123 with Ln=Y, Nd, and La, respectively. The black lines represents fits to the 10 K spectra obtained using the MLM model. The intralayer distance increases by about 8% when going from Y123 (a) through to La123 (c) [38]. Panel (d) shows the spectra of $\sigma_{bil,1}$ inferred from the MLM fitting.

within the lower part of the ARPES error-bar interval. Recall that infrared spectroscopy is a bulk-sensitive technique. As such, our results provide an important validation that the band splitting is indeed a bulk phenomenon rather than a surface effect or a result of a surface modification [25,37].

An alternative way to modify t_{\perp} is via changes of the distance, d_{bl} , between the two closely spaced CuO_2 layers (the intralayer distance). In this case, t_{\perp} is expected to decrease as d_{bl} increases. Experimentally, d_{bl} can be affected by substitutions of the Y ion by Ln^{3+} species with larger ion size, r_{ion} . For example, $r_{ion}(\text{Y}) < r_{ion}(\text{Nd}) < r_{ion}(\text{La})$ leads to La123 having about 8% larger d_{bl} than Y123 [38]. Thus one might expect a lower energy BA mode for La123 as compared to Y123 of a similar doping level. We find that this is indeed the case. Figures 4(a)–4(c) shows the spectra of $\sigma_{c,1}$ along with their respective MLM based fits (black lines) for Ln123 samples with Ln=Y, Nd, and La, all at a similar doping level of $p \approx 0.12$. The inferred spectra of $\sigma_{bil,1}$ shown in Fig. 4(d) are consistent with our expectations from

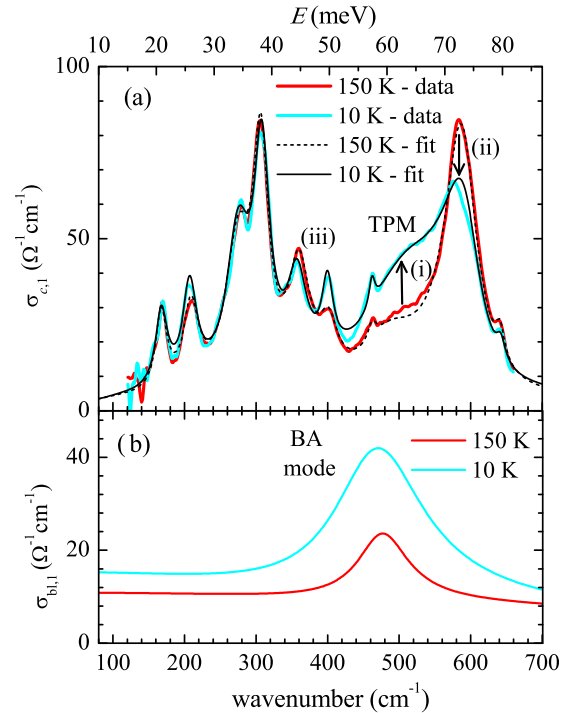


FIG. 5. (a) The real part of the c -axis conductivity of slightly underdoped Bi2223 with $p = 0.132$ and $T_c = 102$ K. Data at 150 K (red line) and 10 K (cyan lines) and fits using the MLM for 150 K (dotted line) and 10 K (black solid line). (b) The real part of $\sigma_{bil}(\omega)$ corresponding to the model spectra shown in panel (a).

the arguments above—the BA mode moves to lower energy as r_{ion} increases from Ln=Y to Nd to La.

D. Bi-based cuprates

We have also analyzed with the MLM the c -axis conductivity of a weakly underdoped Bi-based cuprate superconductor Bi2223 with $T_c = 102$ K, $p = 0.132$, which exhibits a pronounced TPM feature. Figure 5(a) shows the real part of the c -axis conductivity of the Bi2223 single crystal. When compared with the 150 K data (red line), the 10 K data (cyan line) display several significant differences: (i) an increase in spectral weight around 500 cm^{-1} (a TPM feature), (ii) a softening and broadening of the 580 cm^{-1} phonon, and (iii) anomalous changes of the 360 cm^{-1} and 400 cm^{-1} phonons.

The features (i) and (ii) appear qualitatively similar to those for Y123 discussed above and we model them in the same way with the MLM. Next we summarize the important details of our approach. The interbilayer conductivity, $\sigma_{int}(\omega)$, has been set equal to zero since the Bi-O “blocking layers” separating the CuO_2 trilayers are almost insulating. The mode at 580 cm^{-1} is included as usual as an interbilayer oxygen mode (it predominantly involves in-phase c -axis motion of the apical oxygens [39]). The parameters of this phonon were fixed at their high-temperature values and so the anomalous temperature change of this mode is fully accounted for by the changes in $\sigma_{bil}(\omega)$. The anomalous behavior of the 360 cm^{-1} and 400 cm^{-1} phonons was qualitatively interpreted in Ref. [40] in terms of their eigenvectors. For the 360 cm^{-1} (400 cm^{-1}) mode the oxygens in the outer layers and those

TABLE II. Values of the fitting parameters for slightly underdoped Bi2223 entering the model formulas: frequencies (ω_0), plasma frequencies (ω_{pl}), and broadening parameters (γ) of the oscillators obtained by fitting the 150 K and 10 K data.

T (K)	150	10
ϵ_∞	5.7	5.7
σ_{bl} oscillators (cm^{-1})		
ω_0	0	0
ω_{pl}	851	783
γ	1110	664
ω_0	477	472
ω_{pl}	273	533
γ	86	150
High energy interbilayer oxygen phonon mode (cm^{-1})		
ω_0	627	627
ω_{pl}	538	538
γ	48	48
Mean-field phonon modes (cm^{-1})		
ω_0	641	642
ω_{pl}	90	74.6
γ	15	15
ω_0	462	462
ω_{pl}	70	70
γ	15	10
ω_0	401.2	399.8
ω_{pl}	152.1	155.5
γ	29.1	19.1
ω_0	360.1	357.3
ω_{pl}	261.1	231.1
γ	35.8	33.6
ω_0	306.6	307.9
ω_{pl}	309.6	310.3
γ	25.3	26.1
ω_0	275.1	275.2
ω_{pl}	326.2	320.3
γ	43.1	40.1
ω_0	209.1	207.2
ω_{pl}	187.2	199.8
γ	25.2	23.6
ω_0	167.4	167.6
ω_{pl}	160.6	164.4
γ	18.9	20.5

in the central layer vibrate approximately in phase (out of phase). A simple quantitative model of the anomalies of these phonons was elaborated in Ref. [16]. However, the behavior of these phonons in a real material depends very sensitively on details of the eigenvectors and of the local fields and it is thus difficult to include these phonons in the MLM based fit in a rigorous way. We have therefore decided to treat them as responding to the mean electric field rather than to the local fields. The other phonons have been treated in the same way.

The resulting fits are shown in Fig. 5(a) for 150 K (dotted line) and for 10 K (solid black line). Values of the fitting parameters are given in Table II. We see that the model fits the data reasonably well in the critical range between 450–650 cm^{-1} . The corresponding spectra of $\sigma_{bl,1}$ shown in Fig. 5(b) exhibit a well defined mode near 500 cm^{-1} and a broad background. We do not show here the alternative fit with

the Drude peak in $\sigma_{bl}(\omega)$ since this model fails to reproduce the data. It appears that the features (i) and (ii) of the 10 K data listed above are only reasonably reproduced if the resonance in $\sigma_{bl}(\omega)$ is at a finite frequency near 500 cm^{-1} . Note that the frequency of the TPM in $\sigma_{c,1}(\omega)$ is only slightly higher than that of the BA mode in $\sigma_{bl}(\omega)$ in contrast to the case of Y123. This is because for Bi2223, the BA mode has a fairly small spectral weight compared with Y123. As discussed in Appendix, the TPM occurs close to the longitudinal optical frequency of $\sigma_{bl}(\omega)$, which, due to the small spectral weight, is relatively close in this case to the transverse optical frequency.

We note that the sharp structure near 480 cm^{-1} in $\sigma_{bl,1}(\omega)$ at 150 K [see Fig. 5(b)] is probably an artifact due to the fact that the phonons at 360 and 400 cm^{-1} are treated as noninteracting (mean-field) in the model as discussed above. In particular, the sharp dip around 440 cm^{-1} in the spectra of $\sigma_{c,1}$ might be a result of an interference of the phonons with the electronic background. The small peak at 150 K is there essentially to model the small belly around 500 cm^{-1} which may not be there without the dip at 440 cm^{-1} .

Our modeling of the infrared response of Bi2223 thus reveals a BA mode at about 500 cm^{-1} (60 meV) for $p = 0.132$. This value is comparable to the normal-state magnitude of the bonding-antibonding splitting in near optimally doped Bi2212 of ~ 100 meV that is obtained by ARPES near the antinodes in the Brillouin zone [20,41,42]. Note that the splitting is smaller away from the antinodes, with ARPES measurements indicating a value of ~ 15 meV near the nodes [43], and that the energy of the BA mode of Ref. [19] derives from a weighted average of the normal state splitting over all the Brillouin zone. The situation for Bi2223 is somewhat more complicated as the inner- and outer-CuO₂ layers have different values of p , and there are now three bands crossing the Fermi level [23,44]. For Bi2223, Mori *et al.* predict that the value of the bonding-antibonding splitting is about 1.5 times larger than that for the bilayer compound [44]. Generally, the band splitting in ARPES spectra is more pronounced for overdoped samples, where the quasiparticle lifetime is much longer, whereas in our optical conductivity spectra it is more readily identifiable in slightly-underdoped samples, where the TPM feature and phonon anomalies are more pronounced.

IV. SUMMARY

With a phenomenological multilayer model, we have quantitatively analyzed the phonon anomalies occurring in the c -axis conductivity of several high-temperature cuprate superconductors for various values of the hole doping, p . The multilayer model introduces two local conductivities: the conductivity $\sigma_{bl}(\omega)$ of the region between the closely spaced CuO₂ layers (the so-called *intra*-bilayer region) and the local conductivity $\sigma_{int}(\omega)$ of the region separating these stacks of CuO₂ layers (the so-called *inter*-bilayer region).

The modeling of YBa₂Cu₃O_{7- δ} data shows that bilayer splitting is already developed for $p > 0.10 \pm 0.01$, with the superconductivity related maximum in the spectra of the real part of $\sigma_{bl}(\omega)$ centered at a finite energy, increasing from 30 meV at $p = 0.115$ to 55 meV at $p = 0.137$. The results are in good agreement with the theoretical study of the c -axis response of bilayer compounds in Ref. [19] that predicts

a collective intrabilayer mode at a similar energy due to a strong coupling of the two adjacent CuO₂ layers. This mode cannot be assigned to a simple picture of a transition between the bonding and antibonding bands—the latter transitions are instead predicted to manifest themselves at higher energies and have indeed been observed in samples with $p > 0.11$ [19]. For $p = 0.09$, the maximum of $\sigma_{\text{bl},1}(\omega)$ is centered essentially at zero energy which points to a weak (Josephson) coupling. This doping dependence is in agreement with the trends deduced from angle-resolved photoemission data where the onset of a strong intrabilayer coupling (i.e., well resolved bonding and antibonding bands) occurs at $p_c = 0.12 \pm 0.02$ [25], with our results showing that this splitting of the conduction band is indeed a bulk effect.

ACKNOWLEDGMENTS

The authors would like to thank Dr. J. Chaloupka for useful discussions on this work. This work was supported by the Schweizerische Nationalfonds (SNF) through Grant No. 200020-172611 and by the MEYS of the Czech Republic under the project CEITEC 2020 (LQ1601). B.P.P.M. acknowledges support from the Rutherford Foundation of New Zealand. Some measurements were performed at the IR beam line of the ANKA synchrotron at FZ Karlsruhe, where we acknowledge the support of Y.L. Mathis and M. Süpfle.

APPENDIX: FORMULA FOR THE FREQUENCY OF THE BA MODE IN A SIMPLE CASE

Here we derive the formula for the frequency of the BA mode in the most simple case of vanishing interbilayer conductivity and electron-phonon coupling neglected. In the absence of any phonon contribution, the formula for the c -axis dielectric function yielded by the solution of the complete set of equations (see Sec. 4 of Ref. [30]) reads

$$\frac{1}{\epsilon(\omega)} = \frac{z_{\text{bl}}}{\epsilon_{\text{bl}}(\omega)} + \frac{z_{\text{int}}}{\epsilon_{\text{int}}(\omega)}, \quad (\text{A1})$$

where $z_{\text{bl}} = d_{\text{bl}}/(d_{\text{bl}} + d_{\text{int}})$ and $z_{\text{int}} = d_{\text{int}}/(d_{\text{bl}} + d_{\text{int}})$ are the volume fractions of the bilayer and interbilayer region, respectively. Functions $\epsilon_{\text{bl}}(\omega) = \epsilon_{\infty} + \chi_{\text{bl}}(\omega)$ and $\epsilon_{\text{int}}(\omega) = \epsilon_{\infty} + \chi_{\text{int}}(\omega)$ can be viewed as the dielectric functions of the intra- and interbilayer region, respectively. Since the complex

impedance is inversely proportional to the dielectric function, Eq. (A1) can be viewed as the formula for the total impedance of the set of the intrabilayer and interbilayer impedances in series, which was pointed out in the early paper by van der Marel and A. Tsvelkov [17]. If we assume $\chi_{\text{bl}}(\omega)$ in the form of an undamped Lorentzian resonance at frequency ω_{BA} ,

$$\chi_{\text{bl}}(\omega) = \frac{\omega_{\text{bl}}^2}{\omega_{\text{BA}}^2 - \omega^2} \quad (\text{A2})$$

and assume that the interbilayer region is insulating, $\chi_{\text{int}}(\omega) = 0$, Eq. (A1) yields

$$\epsilon(\omega) = \epsilon_{\infty} + \frac{S}{\omega_{\text{TPM}}^2 - \omega^2}, \quad (\text{A3})$$

where

$$\omega_{\text{TPM}}^2 = z_{\text{int}} \frac{\omega_{\text{bl}}^2}{\epsilon_{\infty}} + \omega_{\text{BA}}^2 \quad (\text{A4})$$

and

$$S = z_{\text{bl}} \omega_{\text{bl}}^2. \quad (\text{A5})$$

Since the geometrical factor z_{int} is typically close to 1 in cuprates, the frequency of TPM (A4) is close to the screened longitudinal optical frequency of the intrabilayer dielectric function. Equation (A5) shows that the spectral weight increases with increasing number of CuO₂ planes per unit cell provided ω_{bl} is constant. We express the frequency of the BA mode from Eqs. (A4) and (A5) as

$$\omega_{\text{BA}}^2 = \omega_{\text{TPM}}^2 - \frac{z_{\text{int}} S}{z_{\text{bl}} \epsilon_{\infty}}. \quad (\text{A6})$$

We can see that in the limit of small spectral weight S , the frequency of the BA mode approaches that of the TPM, which is the case of Bi2223 analyzed in this paper. With increasing S , the BA mode frequency decreases, and it can be significantly lower than that of the TPM, as is the case of Y123 with $p = 0.115$ analyzed in Sec. III A. For strongly underdoped Y123 ω_{BA} seems to approach zero. Equation (A6) can be in principle used for a simple estimate of the BA mode frequency from experimental values of ω_{TPM} , S , and ϵ_{∞} , provided that the assumptions are reasonably valid, i.e., the compound is strongly anisotropic ($\chi_{\text{int}}(\omega) \approx 0$) and the interactions with phonons are weak enough. In other cases, a fitting of the data with the full model with interacting phonons is needed.

[1] C. C. Homes, T. Timusk, R. Liang, D. A. Bonn, and W. N. Hardy, *Phys. Rev. Lett.* **71**, 1645 (1993).
 [2] J. Schützmann, S. Tajima, S. Miyamoto, Y. Sato, and R. Hauff, *Phys. Rev. B* **52**, 13665 (1995).
 [3] L. Yu, D. Munzar, A. V. Boris, P. Yordanov, J. Chaloupka, T. Wolf, C. T. Lin, B. Keimer, and C. Bernhard, *Phys. Rev. Lett.* **100**, 177004 (2008).
 [4] C. Bernhard, D. Munzar, A. Golnik, C. T. Lin, A. Wittlin, J. Humlíček, and M. Cardona, *Phys. Rev. B* **61**, 618 (2000).
 [5] T. Timusk and C. Homes, *Solid State Commun.* **126**, 63 (2003).

[6] A. V. Pimenov, A. V. Boris, L. Yu, V. Hinkov, T. Wolf, J. L. Tallon, B. Keimer, and C. Bernhard, *Phys. Rev. Lett.* **94**, 227003 (2005).
 [7] A. Dubroka, M. Rössle, K. W. Kim, V. K. Malik, D. Munzar, D. N. Basov, A. A. Schafgans, S. J. Moon, C. T. Lin, D. Haug, V. Hinkov, B. Keimer, T. Wolf, J. G. Storey, J. L. Tallon, and C. Bernhard, *Phys. Rev. Lett.* **106**, 047006 (2011).
 [8] E. Uykur, K. Tanaka, T. Masui, S. Miyasaka, and S. Tajima, *Phys. Rev. Lett.* **112**, 127003 (2014).
 [9] C. Homes, T. Timusk, D. Bonn, R. Liang, and W. Hardy, *Physica C (Amsterdam)* **254**, 265 (1995).

- [10] C. Homes, T. Timusk, D. Bonn, R. Liang, and W. Hardy, *Can. J. Phys.* **73**, 663 (1995).
- [11] W. Hu, S. Kaiser, D. Nicoletti, C. R. Hunt, I. Gierz, M. C. Hoffmann, M. Le Tacon, T. Loew, B. Keimer, and A. Cavalleri, *Nat. Mater.* **13**, 705 (2014).
- [12] C. Giannetti, M. Capone, D. Fausti, M. Fabrizio, F. Parmigiani, and D. Mihailovic, *Adv. Phys.* **65**, 58 (2016).
- [13] W. Hu, D. Nicoletti, A. V. Boris, B. Keimer, and A. Cavalleri, *Phys. Rev. B* **95**, 104508 (2017).
- [14] D. Munzar, C. Bernhard, A. Golnik, J. Humlíček, and M. Cardona, *Solid State Commun.* **112**, 365 (1999).
- [15] V. Železný, S. Tajima, D. Munzar, T. Motohashi, J. Shimoyama, and K. Kishio, *Phys. Rev. B* **63**, 060502 (2001).
- [16] A. Dubroka and D. Munzar, *Physica C (Amsterdam)* **405**, 133 (2004).
- [17] D. van der Marel and A. Tsvetkov, *Czech. J. Phys.* **46**, 3165 (1996).
- [18] S. V. Dordevic, E. J. Singley, J. H. Kim, M. B. Maple, S. Komiya, S. Ono, Y. Ando, T. Rōm, R. Liang, D. A. Bonn, W. N. Hardy, J. P. Carbotte, C. C. Homes, M. Strongin, and D. N. Basov, *Phys. Rev. B* **69**, 094511 (2004).
- [19] J. Chaloupka, C. Bernhard, and D. Munzar, *Phys. Rev. B* **79**, 184513 (2009).
- [20] Y.-D. Chuang, A. D. Gromko, A. Fedorov, Y. Aiura, K. Oka, Y. Ando, H. Eisaki, S. I. Uchida, and D. S. Dessau, *Phys. Rev. Lett.* **87**, 117002 (2001).
- [21] D. L. Feng, N. P. Armitage, D. H. Lu, A. Damascelli, J. P. Hu, P. Bogdanov, A. Lanzara, F. Ronning, K. M. Shen, H. Eisaki, C. Kim, Z.-X. Shen, J.-i. Shimoyama, and K. Kishio, *Phys. Rev. Lett.* **86**, 5550 (2001).
- [22] A. Damascelli, Z. Hussain, and Z.-X. Shen, *Rev. Mod. Phys.* **75**, 473 (2003).
- [23] S. Ideta, K. Takashima, M. Hashimoto, T. Yoshida, A. Fujimori, H. Anzai, T. Fujita, Y. Nakashima, A. Ino, M. Arita, H. Namatame, M. Taniguchi, K. Ono, M. Kubota, D. Lu, Z.-X. Shen, K. Kojima, and S. Uchida, *Physica C (Amsterdam)* **470**, 14 (2010).
- [24] M. Hossain, J. Mottershead, D. Fournier, A. Bostwick, J. McChesney, E. Rotenberg, R. Liang, W. Hardy, G. Sawatzky, I. Elfimov, D. Bonn, and A. Damascelli, *Nat. Phys.* **4**, 527 (2008).
- [25] D. Fournier, G. Levy, Y. Pennec, J. McChesney, A. Bostwick, E. Rotenberg, R. Liang, W. Hardy, D. Bonn, I. Elfimov, and A. Damascelli, *Nat. Phys.* **6**, 905 (2010).
- [26] S. V. Borisenko, A. A. Kordyuk, V. Zabolotnyy, J. Geck, D. Inosov, A. Koitzsch, J. Fink, M. Knupfer, B. Büchner, V. Hinkov, C. T. Lin, B. Keimer, T. Wolf, S. G. Chiuzbăian, L. Patthey, and R. Follath, *Phys. Rev. Lett.* **96**, 117004 (2006).
- [27] S. Schlachter, W. Fietz, K. Grube, T. Wolf, B. Obst, P. Schweiss, and M. Kläser, *Physica C (Amsterdam)* **328**, 1 (1999).
- [28] R. Azzam, N. Bashara, and S. Ballard, *Ellipsometry and Polarized Light* (North Holland, New York, 1977).
- [29] C. Bernhard, J. Humlíček, and B. Keimer, *Thin Solid Films* **455**, 143 (2004).
- [30] A. Dubroka, L. Yu, D. Munzar, K. Kim, M. Rössle, V. Malik, C. Lin, B. Keimer, T. Wolf, and C. Bernhard, *Eur. Phys. J.-Special Topics* **188**, 73 (2010).
- [31] J. Vašátko and D. Munzar, *Phys. Rev. B* **86**, 014512 (2012).
- [32] M. Grüninger, D. van der Marel, A. Damascelli, A. Erb, T. Nunner, and T. Kopp, *Phys. Rev. B* **62**, 12422 (2000).
- [33] J. R. Schrieffer, *Theory of Superconductivity* (Addison-Wesley, Boston, 1988).
- [34] N. Bogoljubov, V. V. Tolmachev, and D. Širkov, *Fortschr. Phys.* **6**, 605 (1958).
- [35] P. W. Anderson, *Phys. Rev.* **110**, 827 (1958).
- [36] Y. Hirata, K. M. Kojima, M. Ishikado, S. Uchida, A. Iyo, H. Eisaki, and S. Tajima, *Phys. Rev. B* **85**, 054501 (2012).
- [37] A. D. Palczewski, T. Kondo, J. S. Wen, G. Z. J. Xu, G. Gu, and A. Kaminski, *Phys. Rev. B* **81**, 104521 (2010).
- [38] M. Guillaume, P. Allenspach, W. Henggeler, J. Mesot, B. Roessli, U. Staub, P. Fischer, A. Furrer, and V. Trounov, *J. Phys.: Condens. Matter* **6**, 7963 (1994).
- [39] N. N. Kovaleva, A. V. Boris, T. Holden, C. Ulrich, B. Liang, C. T. Lin, B. Keimer, C. Bernhard, J. L. Tallon, D. Munzar, and A. M. Stoneham, *Phys. Rev. B* **69**, 054511 (2004).
- [40] A. V. Boris, D. Munzar, N. N. Kovaleva, B. Liang, C. T. Lin, A. Dubroka, A. V. Pimenov, T. Holden, B. Keimer, Y.-L. Mathis, and C. Bernhard, *Phys. Rev. Lett.* **89**, 277001 (2002).
- [41] A. Kaminski, S. Rosenkranz, H. M. Fretwell, Z. Z. Li, H. Raffy, M. Randeria, M. R. Norman, and J. C. Campuzano, *Phys. Rev. Lett.* **90**, 207003 (2003).
- [42] Y.-D. Chuang, A. D. Gromko, A. V. Fedorov, Y. Aiura, K. Oka, Y. Ando, M. Lindroos, R. S. Markiewicz, A. Bansil, and D. S. Dessau, *Phys. Rev. B* **69**, 094515 (2004).
- [43] T. Yamasaki, K. Yamazaki, A. Ino, M. Arita, H. Namatame, M. Taniguchi, A. Fujimori, Z.-X. Shen, M. Ishikado, and S. Uchida, *Phys. Rev. B* **75**, 140513 (2007).
- [44] M. Mori, T. Tohyama, and S. Maekawa, *Phys. Rev. B* **66**, 064502 (2002).
- [45] R. Henn, T. Strach, E. Schönherr, and M. Cardona, *Phys. Rev. B* **55**, 3285 (1997).